DESIGN STUDY OF A TIME OF FLIGHT SMALL-ANGLE DIFFRACTOMETER FOR A PULSED NEUTRON SOURCE

J.M. Carpenter and J. Faber, Jr.

CONF-771077-4

Prepared for

4th International Conference on
Small-Angle Scattering of
X-rays and Neutrons
Gatlinburg, TN
October 3-7, 1977

U of C-AUA-USERDA

ARGONNE NATIONAL LABORATORY, ARGONNE, ILLINOIS

operated under contract W-31-109-Eng-38 for the
U. S. ENERGY RESEARCH AND DEVELOPMENT ADMINISTRATION

Design Study of a Time of Flight Small-Angle Diffractometer for a Pulsed Neutron Source*

J. M. Carpenter and J. Faber, Jr.

Argonne National Laboratory, Argonne, Illinois 60439

ABSTRACT

The present design study for a neutron SAS instrument at Argonne's proposed Intense Pulsed Neutron Source (peak thermal neutron flux 10^{16} n/cm^2-sec) indicates that an effective high-resolution TOF SAS diffractometer can be constructed. The design features include a converging slit collimator, provision for 5 x 5 cm^2 sample cross sectional area, and a 1 x 1 m^2, two-dimensional detector. The fractional wavelength resolution of the instrument is negligibly small for all wavelengths. The resolution was computed by Monte Carlo simulation and is constant over most of the Q range. A special feature of the instrument is the wide range of accessible Q 's, without the requirement of instrument configurational changes. The flux on sample exceeds that at conventional reactor instruments of comparable resolution.

*Based on work performed under the auspices of the U. S. Energy Research and Development Administration.

INTRODUCTION

In this paper, we present the design study of a neutron small-angle scattering (SAS) instrument for use at Argonne's proposed Intense Pulsed Neutron Source (Carpenter & Werner, 1976; Werner, 1977; Carpenter, 1977.) The instrument design incorporates several unique features: a converging-slit collimator, wavelength band-limiting choppers, capacity for large samples, and a two dimensional detector. Machine design-dependent parameters are considered in a Monte-Carlo code that produces estimates of the instrumental resolution function and available flux at the sample. We find that the flux on sample exceeds that at steady-state reactor instruments of comparable resolution.

Pulsed neutron sources can provide higher effective neutron fluxes than are available at high-flux research reactors (e.g., the peak thermal flux at IPNS is 10^{16} n/cm^2-sec). Time of flight (TOF) techniques must be employed in neutron scattering measurements in order to exploit pulsed neutron sources efficiently. These techniques have been developed for many applications at pulsed sources and at steady-state reactors (using choppers). Although the first neutron SAS experiments (Krueger, et al. 1949) used TOF techniques, most measurements currently performed use very efficient instruments based on steady-state monochromatic neutron beams. The increasing need for neutron SAS instrumentation and the advent of next-generation pulsed sources dictate the further development of neutron SAS facilities. Recently, at Dubna (Cser, 1975) and Harwell (Mildner & Windsor, 1977), TOF instruments have been tested at pulsed neutron sources. An excellent contrast of pulsed and steady-state SAS instruments has been presented (Mildner, 1977).

INSTRUMENT SCHEMATICS

A schematic design of the neutron instrument is shown in Fig. 1, and appears to resemble a steady state source instrument. However, in the steady-state instrument, the incident wavelength λ_0 is fixed by a crystal or drum velocity selector and a range of wave vector change $Q = \frac{4\pi \sin\theta}{\lambda}$ is scanned by use of an array of detectors. In the time of flight instrument, a wide range of incident wavelengths is used, and the time at which neutrons started at the pulsing device is known. Neutrons are sorted by wavelength according to their time of flight $t = (m/h(L_1 + L_2(\theta))\lambda$ across the known path $(L_1 + L_2(\theta))$ and the wave vector change Q for each wavelength λ is determined for each direction θ. Since each detector direction corresponds to a range of $Q = \frac{4\pi \sin\theta}{\lambda}$, $(\cos 2\theta = \underline{\Omega}_i \cdot \underline{\Omega}_f)$ and a wide band of wavelengths is used, the time of flight instrument spans a greater range of Q than a steady state instrument with the same angular range. The intensity however has a substantially different dependence on Q. In the following discussion, we shall examine various components of the instrument design.

MULTIPLE-CONVERGING-SLIT COLLIMATOR

In Figure 2, a point on the detector $\underline{R}_D$ (measured from the center of the detector) defines a nominal change in neutron direction $\underline{\Omega}_{fo}$ relative to the instrument centerline $\underline{\Omega}_{io}$, which is $\Delta\underline{\Omega}_o = \underline{\Omega}_{fo} - \underline{\Omega}_{io} \cong \frac{\underline{R}_D}{L_2}$. The incident direction defined by a collimating channel whose centerline passes through $\underline{R}_M$ and $\underline{R}_S$ on the moderator and sample is $\underline{\Omega}_i \cong \frac{\underline{R}_S - \underline{R}_M}{L_1}$. The scattered neutron direction defined by a point at $\underline{R}_S$ on the sample and $\underline{R}_D$ on the detector is $\underline{\Omega}_f \cong \frac{\underline{R}_D - \underline{R}_S}{L_2}$, so that the change in direction is

$$\Delta\underline{\Omega} = \underline{\Omega}_f - \underline{\Omega}_i \tag{1}$$

$$\cong \Delta\underline{\Omega}_o - \underline{R}_S \left(\frac{1}{L_2} + \frac{1}{L_1}\right) - \frac{\underline{R}_M}{L_1} \quad . \tag{2}$$

If the centers of collimating channels are arranged so that

$$\underline{R}_M = \frac{L_1 + L_2}{L_2} \underline{R}_S \tag{3}$$

then the second term in $\Delta\underline{\Omega}$ vanishes, and

$$\Delta\underline{\Omega} = \Delta\underline{\Omega}_o \qquad \text{independently of } \underline{R}_M, \underline{R}_S \quad . \tag{4}$$

The displaced collimating channel acts indentically to the central collimating channel.

The condition $\underline{R}_M = \frac{L_1 + L_2}{L_2} \underline{R}_S$ is interpreted geometrically in Fig. 2: $\underline{R}_M$ and $\underline{R}_S$ lie on a line passing through the center of the detector. Thus a two-dimensional collimating system consisting of channels which converge at a point on the detector may be used to increase the area of source and sample which can be used in a small angle scattering instrument.

The relations between sample and detector element sizes

$$Y_S = \frac{L_1}{L_1 + L_2} Y_D \quad , Z_S = \frac{L_1}{L_1 + L_2} Z_D \tag{5}$$

produce an optimized counting rate,[5] and the relations

$$Y_M = \frac{L_1 + L_2}{L_2} Y_S, \quad Z_M = \frac{L_1 + L_2}{L_2} Z_S \tag{6}$$

provide collimating elements arranged to satisfy Eq. (3). The collimator for the present instrument might be constructed from B^{10} filaments, stacked in rectangular arrays (Nunes, 1977).

BASIC DESIGN

The resolution of a time of flight diffractometer can be expressed as

$$\left(\frac{\Delta Q}{Q}\right)^2 = \left(\frac{\Delta t}{t}\right)^2_{Source} + \left(\frac{\Delta t}{t}\right)^2_{Geom} + \left(\frac{\Delta t}{t}\right)^2_{Det} \quad , \qquad (7)$$

where the $(\Delta t/t)_i$ are the contribution from source pulse width, the geometric contribution, and the contribution from detection time uncertainty. The source pulse width contribution $(\Delta t/t)_{Source} = v\Delta t/L$; $v\Delta t$ is roughly independent of λ and equal to about .1 m. Since the length of the time analysis path $L = L_1 + L_2$ is of the order of ten meters, $(\Delta t/t)_{Source} \lesssim \frac{.1}{10} = .01$. This is much smaller than the desired overall resolution and can be ignored for purposes of rough design. Similarly $(\Delta t/t)_{Detector}$ contains a part due to detector thickness, a few centimeters, and a part due to detector pulse time jitter, a few microseconds at most. Thus $(\Delta t/t)_{Det}$ also can be ignored for purposes of rough design.

The dominant contribution to the overall resolution is $(\Delta t/t)_{Geom}$, which can be written

$$\left(\frac{\Delta t}{t}\right)_{Geom} = \left(\frac{\Delta\theta}{\theta}\right) = \frac{4\pi}{\lambda Q} \quad . \qquad (8)$$

Considering scattering in a plane parallel to the y edges of the detector, sample, and moderator apertures (see Fig. 1),

$$\Delta\theta_y^2 = 8\ \ell n2\ (\frac{1}{12})\ (\frac{1}{4})\ [\frac{Y_M^2}{L_1^2} + Y_S^2\ (\frac{1}{L_1} + \frac{1}{L_2})^2 + \frac{Y_D^2}{L_2^2}] \quad ; \qquad (9)$$

The factor $8\ell n2$ relates $(FWHM)^2$ to variance as though the angular distribution were gaussian (it is actually slightly narrower).

Using Eqs. (5) and (6),

$$\Delta\theta_y = \sqrt{\frac{\ell n2}{2}}\ \frac{Y_D}{L_2} \quad . \qquad (10)$$

Similarly for Z_M, Z_S, Z_D. Y_D is fixed by currently available detector technology, i.e., $Y_D = Z_D \sim 0.5$ cm. Since $\theta = \lambda Q/(4\pi)$ and $\Delta\theta = \theta(\Delta Q/Q)$, if ΔQ is established and a nominal wavelength chosen, L_2 is given by

$$L_2 = \sqrt{\frac{\ell n2}{2}}\ \frac{Y_D}{\Delta\theta_y} = \sqrt{\frac{\ell n2}{2}}\ \frac{4\pi Y_D}{\lambda\Delta Q} \quad . \qquad (11)$$

For purposes of rough design, the length of the initial path L_1 and therefore Y_M and Y_S have not been established according to optimum principles. Since the ratio Y_M/L_1 is established by the resolution requirements, the flux at the sample position is independent of L_1 apart from the area lost in the collimator due to the finite dimensions of the collimator wires. L_1 must be greater than the shield radius, about 5 m, and simultaneously L_1 must be short enough to avoid losses due to the need to reduce frequency or wavelength range while respecting frame overlap constraints. The condition to avoid frame overlap is

$$(\frac{m}{h})(L_1 + L_2)(\lambda_{max} - \lambda_{min}) < \frac{1}{f_c} \quad , \qquad (12)$$

where f_c is the frequency of pulses arriving at the sample. The wavelength range should be great enough to enable a large range of Q to be covered in a single run. The frequency of pulses and the wavelength range are established by choppers which run at a submultiple of the source frequency, $f_c = f_s/\text{integer}$. The neutron time schedule of a low resolution instrument is illustrated in Fig. 3. In addition, the chopper must be arranged so that while passing wavelength λ_{max} from the previous pulses it is closed when the next source pulse occurs. The time schedule in Fig. 3 features the use of two choppers at L_{C1} and L_{C2}. The idea is to use one chopper to reduce the source pulse frequency and the other to shape the wavelength band to a particular experimental need.

To establish $(\Delta t/t)_{Geom}$ more precisely as a function of position on the detector, the diffractometer was simulated using Monte Carlo techniques. The calculation accounted for all channels of the multiple channel converging collimator (although irrelevant by the arguments above), for angular uncertainties due to finite moderator, sample, and detector elements, and for a detector .03 m thick. The resolution was fitted to a function of the form

$$\frac{\Delta Q}{Q} = \frac{(A_1 + A_2 Y_{DO}^2 + A_3 Z_{DO}^2 + A_4 Y_{DO}^2 Z_{DO}^2)^{1/2}}{(Y_{DO}^2 + Z_{DO}^2)} \quad . \tag{13}$$

We attach no particular significance to the form of Eq. (15) apart from the observation that it does fit the data very well (residuals $\lesssim$ 0.03).

Rough design parameters were established according to Eq. (11) and resolution refined by the procedure above. The importance of the rough estimates is that they provide important starting-points for the design. The results of applying these design criteria are illustrated in Table I. Three different forms of a SAS instrument are shown.

Table I

Design Parameters of IPNS Small-Angle Diffractometer

Parameters	High Resolution	Medium Resolution	Low Resolution
L_1(m)	10	8	6
L_2(m)	30	8	5
$Y_M = Z_M$ (cm)	0.167	0.5	0.55
$W_M = H_M$ (cm)	10	10	10
$Y_S = Z_S$ (cm)	0.125	0.25	0.273
$W_S = H_S$ (cm)	7.5	5	5
$Y_D = Z_D$ (cm)	0.5	0.5	0.5
$W_D = H_D$ (cm)	100	100	100
Sample Area A_s (cm^2)	56	25	25
ΔQ ($Å^{-1}$)	$\sim 2 \times 10^{-4}$	$\sim 7 \times 10^{-4}$	$\sim 1.4 \times 10^{-3}$
Q_{min} ($Å^{-1}$)	10^{-4}	6×10^{-4}	8×10^{-4}
Q_{max} ($Å^{-1}$)	0.05	0.3	0.2
λ_{max} ($Å^{-1}$)	12	10	15
λ_{min}	2.4	2	3
Chopper freq., f_C (Hz)	10	30	30
Flux on Sample, $\bar{\Phi}_S$ (neutrons/cm^2-sec)	6×10^3	2.6×10^5	5×10^5
D11A, $\bar{\Phi}_S$ @ ΔQ	2×10^3 @ 2×10^{-4}	5×10^4 @ 1×10^{-3}	1.2×10^5 @ 1.4×10^{-3}

The pulsed source instrument, which uses a broad wavelength band, must likely be arranged vertically, since neutrons traveling horizontally would fall a vertical distance $d = \frac{1}{2} g(\frac{m}{h})^2 L^2 \lambda^2 = 3.1$ mm for $\lambda = 10$ Å and L = 10 m.

COUNTING RATE DISTRIBUTION AND AVERAGE RESOLUTION

For a TOF SAS diffractometer and an isotropic material, the time-average counting rate per unit wavelength in the i^{th} detector element is

$$C_i(\lambda) = A_s\, \overline{\Phi}(\lambda)\, \eta(\lambda)\, nd\, \frac{\partial\sigma}{\partial\Omega}(Q)\, \Delta\Omega_i \quad , \tag{14}$$

where A_s is the sample area, $\overline{\Phi}(\lambda)$ the flux per unit wavelength on sample, $\eta(\lambda)$ the detector efficiency, n the number density of scattering units, d the sample thickness, $\partial\sigma/\partial\Omega(Q)$ the scattering cross section per unit solid angle for one scattering unit, and $\Delta\Omega_i$ the solid angle subtended by the i^{th} detector element from the sample. For the i^{th} detector, $Q = 4\pi\theta_i/\lambda$. A useful characterization of the intensity distribution is the counting rate in the i^{th} detector element per unit wavelength per unit scattering probability of the sample $A_s nd\partial\sigma/\partial\Omega$, per unit area of sample:

$$c_i(\lambda) = \frac{C_i(\lambda)}{A_s nd\, \frac{\partial\sigma}{\partial\Omega}(Q)} = \overline{\Phi}(\lambda)\eta(\lambda)\ \Delta\Omega_i \quad . \tag{15}$$

Data can be sorted according to Q-intervals. If all detector elements and wavelengths are included for which the resolution Q is acceptable, then the total, acceptable counting rate per unit Q per unit scattering probability is

$$g(Q,\Delta Q_{Max}(Q)) = \sum_{\substack{i \\ \text{(detector} \\ \text{elements)}}} \int_{\lambda_{min}}^{\lambda_{max}} U[\Delta Q_i(Q) \leq \Delta Q_{Max}(Q)] \times c_i(\lambda)\delta(Q - \frac{2\pi\theta_i}{\lambda})\, d\lambda \tag{16}$$

$$= \sum_i U[\Delta Q_i(Q) \leq \Delta Q_{Max}(Q)]\; U[\lambda_{min} \leq \lambda] U[\lambda \leq \lambda_{max}]\; c_i(\lambda)\, \frac{\lambda}{Q}\Bigg|_{\lambda = \frac{2\pi\theta_i}{Q}} \quad , \tag{17}$$

$$\text{where } U[x < y] = \begin{cases} 1; & x \leq y \\ 0; & x > y \end{cases} \quad .$$

Here, the function $\Delta Q_{Max}(Q)$ is a user-specified function defining the maximum acceptable resolution, $\Delta Q \leq \Delta Q_{Max}(Q)$. C(Q), the counting rate per unit Q in a measurement can then be obtained from $g(Q,\Delta Q_{Max}(Q))$

$$C(Q) = g(Q,\Delta Q_{Max}(Q))\; A_s\; nd\; \frac{\partial\sigma}{\partial\Omega}\,(Q) \quad . \tag{18}$$

We define the function $g(Q, \Delta Q_{Max}(Q))$, as the "diffractometer weight function;" it has the shape of the observed intensity distribution if $\frac{\partial\sigma}{\partial\Omega}(Q)$ = constant. The average resolution width, when $\Delta Q_{Max}(Q)$ is specified, has been estimated as

$$\Delta Q(Q) = \{\sum_i U[\Delta Q_i(Q) \leq \Delta Q_{Max}(Q)]\; U[\lambda_{min} \leq \lambda] U[\lambda \leq \lambda_{max}] c_i(\lambda) \frac{\lambda}{Q}\Bigg|_{\lambda = \frac{2\pi\theta_i}{Q}} (\Delta Q_i(Q))\} \times$$

$$\times\; [g(Q,\Delta Q_{Max}(Q))]^{-1} \; . \tag{19}$$

Figures 4 and 5 show the results of diffractometer weight function and average resolution calculations for two instrument configurations, when no resolution requirements are imposed on the sorting. The actual Q resolution was computed according to Eq. (7), $(v\Delta t)_{Source} = .1$ m, $(v\Delta t)_{Det} = .03$ m. The detector was assumed to be 3 cm thick filled with 2 atm He^3. The time-average flux on sample was represented as

$$\overline{\Phi}(\lambda) = \overline{i}\,(\lambda)/L_1^{\,2} \quad , \tag{20}$$

where

$$\overline{i}(\lambda) = \frac{\Delta A_M}{A_M}\;\frac{f_c}{f_s}\;\overline{S}_N\;EI(E)|_{1\ eV}\;\frac{I(E)}{EI(E)|_{1\ eV}}\cdot\frac{2E}{\lambda} \quad , \tag{21}$$

$$\frac{I(E)}{EI(E)|_{1\ eV}} = \frac{I_{Th}}{EI(E)|_{1\ eV}}\;\frac{E}{E_T^{\,2}}\;e^{-E/E_T} + \frac{1}{E}\,\frac{\Delta_2(E)}{\Delta_2\,(1\ eV)} \quad , \tag{22}$$

and $\Delta_2(E)$ is Wescott's joining function

$$\Delta_2(E) = \frac{1}{1 + \left(\frac{4.95\ E_T}{E}\right)^7} \quad . \tag{23}$$

$\Delta A_M = Y_M Z_M$ is the cross-sectional area at the moderator of a single collimating element and A_M is the total cross-section area of the moderator. $\overline{S}_N$ is the time average source neutron production rate, n/sec, $EI(E)|_{1\ eV}$ is the epithermal beam current per source neutron, n/ster-source n, and $I(E)/EI(E)|_{1\ eV}$ is the normalized spectral shape for the moderator, $I_{Th}/EI(E)|_{1\ eV}$ is the thermal-to-epithermal flux ratio for the moderator and E_T is the moderator spectral temperature. For IPNS II, the time-average neutron production rate $S_N = 9 \times 10^{16}$ source n/sec, the pulse frequency $f_s = 60$ Hz, and $EI(E)|_{1\ eV} = 2.3 \times 10^{-4}$ n/ster-source n (an appropriate moderator in location B of IPNS).

Using $$\frac{I_{Th}}{EI(E)|_{1\ eV}} = 5.9, \text{ and } E_T = .002 \text{ eV } (T = 24 \text{ K})$$

as for a 20 K solid CH_4 moderator, we have evaluated the flux on sample. The results appear in Table I. Table I compares fluxes of the IPNS instruments against those of the ILL D-11A instrument operated at equivalent resolution.

SUMMARY

We have presented a description of TOF neutron SAS design calculations for application at a pulsed source, and reported conceptual designs for three instruments of different resolution at the Intense Pulsed Neutron Source. The formalism can be easily specialized to accommodate a particular set of sample dependent requirements. Apart from the conceptual design however, a number of technical problems must be solved. The experimental area may have a high epithermal background during pulses which must be dealt with when an instrument is operated at a submultiple of the source frequency. The effects of gravity on the neutron trajectory could be minimized by a vertical instrument orientation. Care and attention to detail will be needed to optimize the complex collimating system. The two-dimensional detector specified in the design requires an extension of existing technology. Data sorting, storage and display will require careful planning.

On the other hand, we have demonstrated the wide range of Q that is accessible in a single instrument setup. The flux on sample exceeds that at the

ILL D-11A SAS diffractometer. In Fig. 3, a multiple disk chopper (with phasing) at L_{C2} would allow the experimenter precise control of the wavelength range of interest. In particular, a relatively narrow range of incident neutron energies would allow for the possibility of inelastic scattering experiments. Prototype experiments are planned to test the ideas presented here.

We are pleased to acknowledge a number of illuminating discussions with G. Kostorz during his visit at Argonne.

REFERENCES

Carpenter, J. M. and Werner, S. A. (1976). ANL-76-10 Vol. 2. Uses of Advanced Pulsed Neutron Sources, Report of a Workshop held at Argonne National Laboratory, October 21-24, 1975.

Carpenter, J. M. (1977). To be published in Nuclear Instruments and Methods.

Cser, L. (1975). BNL-50453. Neutron Scattering for the Analysis of Biological Structures, pp. VII.3 - VII.29, Symposium at Brookhaven National Laboratory, 1975.

Mildner, D. F. R. (1977). Private communication, submitted for publication to Nuclear Instruments and Methods.

Nunes, A. C. (1977). See paper in this conference.

Werner, S. A. (1977). NS-24 Proc. 1977 IEEE Particle Accelerator Conference, Chicago, Illinois, March, 1977.

Krueger, H. H. A.; Meneghetti, D; Ringo, G. R. and Windsberg, L. (1949). Phys. Rev. 75, 1098 (1949).

Mildner, D. F. R. and Windsor, C. G. (1977). In preparation.

FIGURE CAPTIONS

Figure 1: Schematic diagram of IPNS Small-Angle Diffractometer. The collimating system is represented only by entrance and exit apertures, but channels are assumed to be continuously defined.

Figure 2: Geometrical Interpretation of conditions for Multiple Converging Slit Collimation.

Figure 3: Neutron time schedule for the TOF Small-Angle Diffractometer (low resolution design). See Table I for design parameters.

Figure 4: Diffractometer Weight Function, $g(Q,\Delta Q_{max})$ and Resolution, $\overline{\Delta Q}$ (approximately constant) as a function of Q for the Low Resolution Instrument. See Eq. (16-17) and Eq. (19).

Figure 5: Diffractometer Weight Function, $g(Q,\Delta Q_{max})$ and Resolution, $\overline{\Delta Q}$ (approximately constant) as a function of Q for the Medium Resolution Instrument. See Eq. (16-17) and Eq. (19).

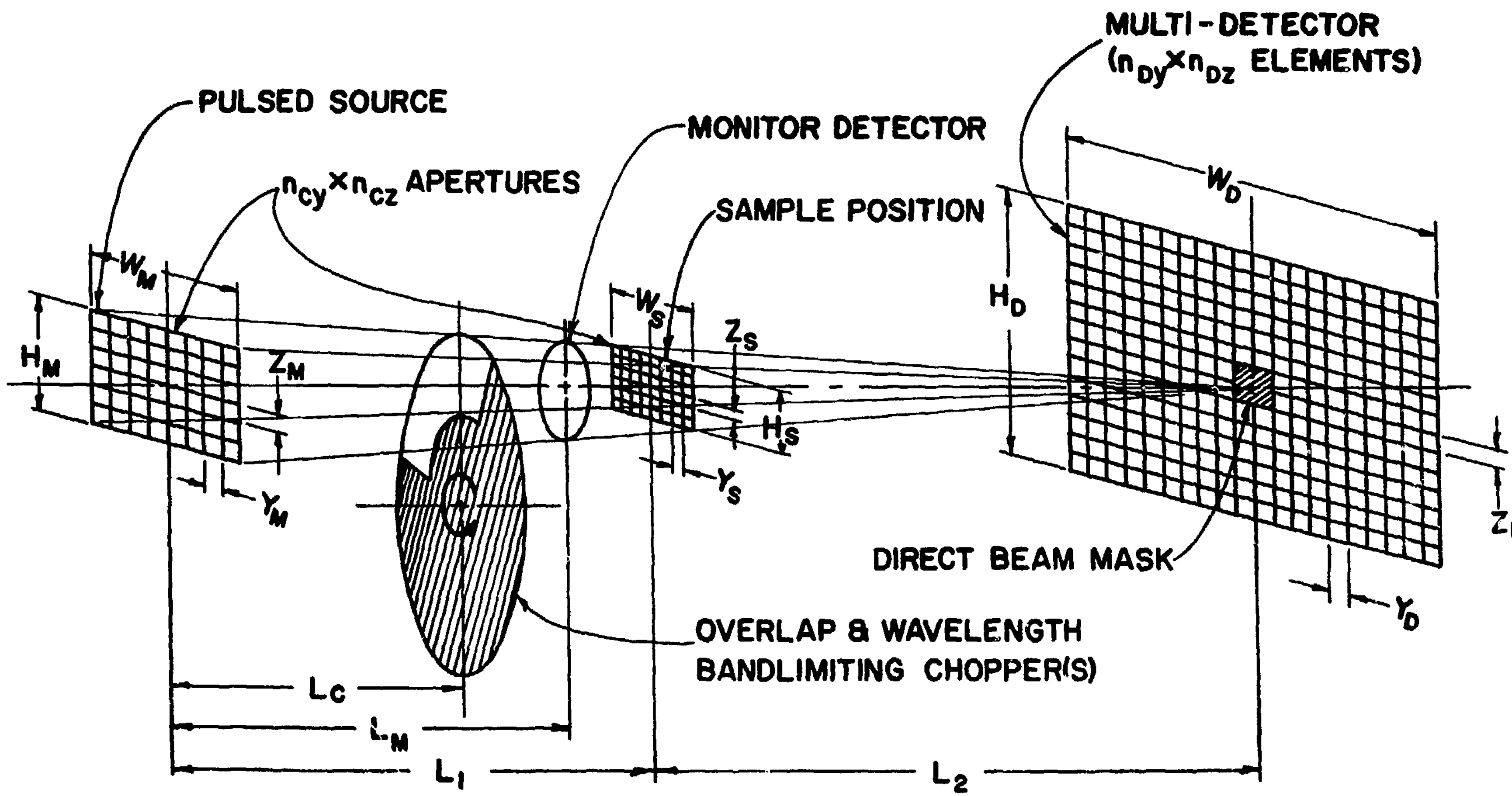

MULTI-DETECTOR
($n_{Dy} \times n_{Dz}$ ELEMENTS)
PULSED SOURCE
MONITOR DETECTOR
$n_{cy} \times n_{cz}$ APERTURES
SAMPLE POSITION
W_D
W_M
W_S
H_D
H_M
Z_M
Z_S
H_S
Y_S
Y_M
Z_D
DIRECT BEAM MASK
Y_D
OVERLAP & WAVELENGTH
BANDLIMITING CHOPPER(S)
L_C
L_M
L_1
L_2

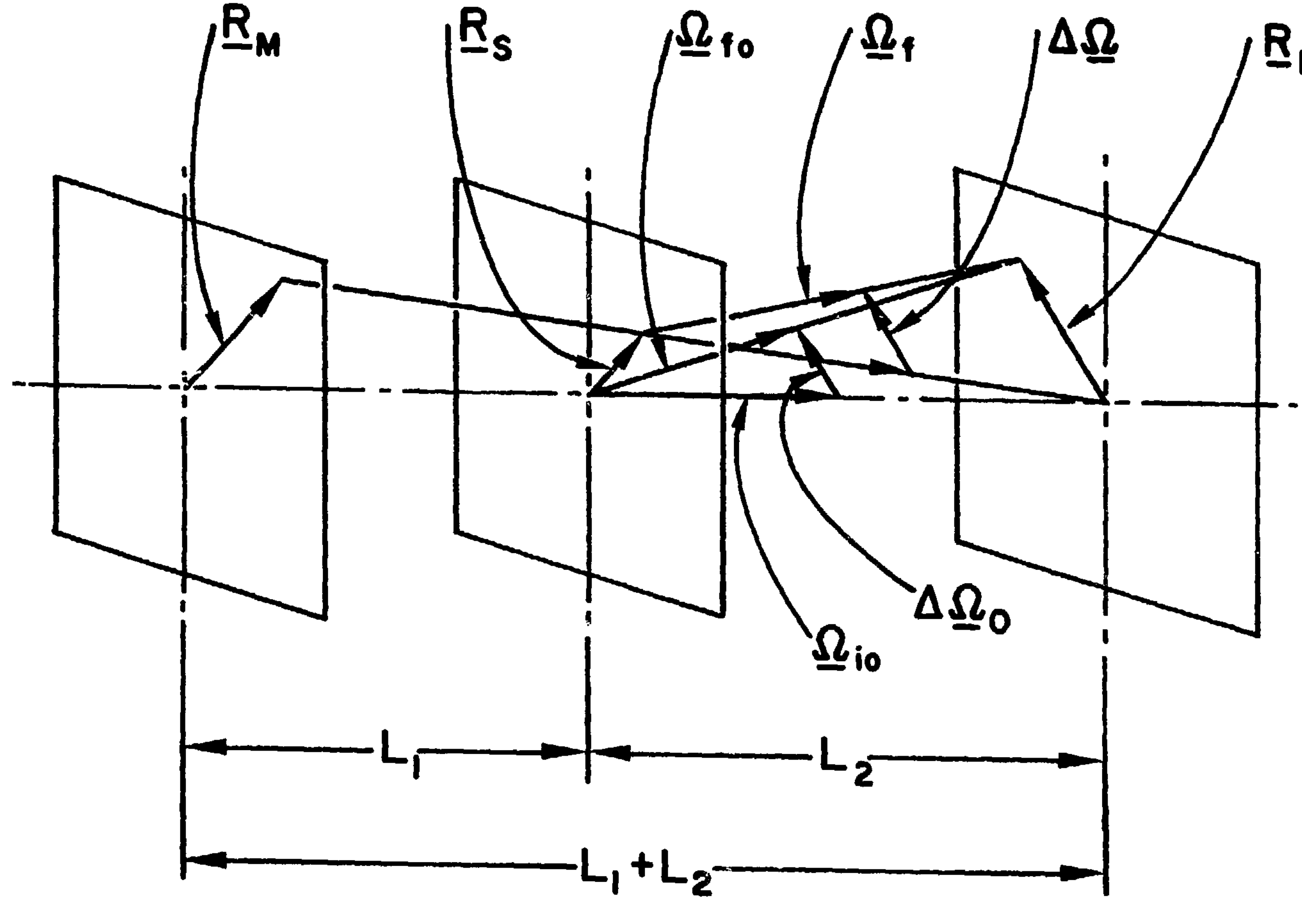
R_M
R_S
Ω_fo
Ω_f
ΔΩ
R_D
ΔΩ_o
Ω_io
L_1
L_2
L_1+L_2

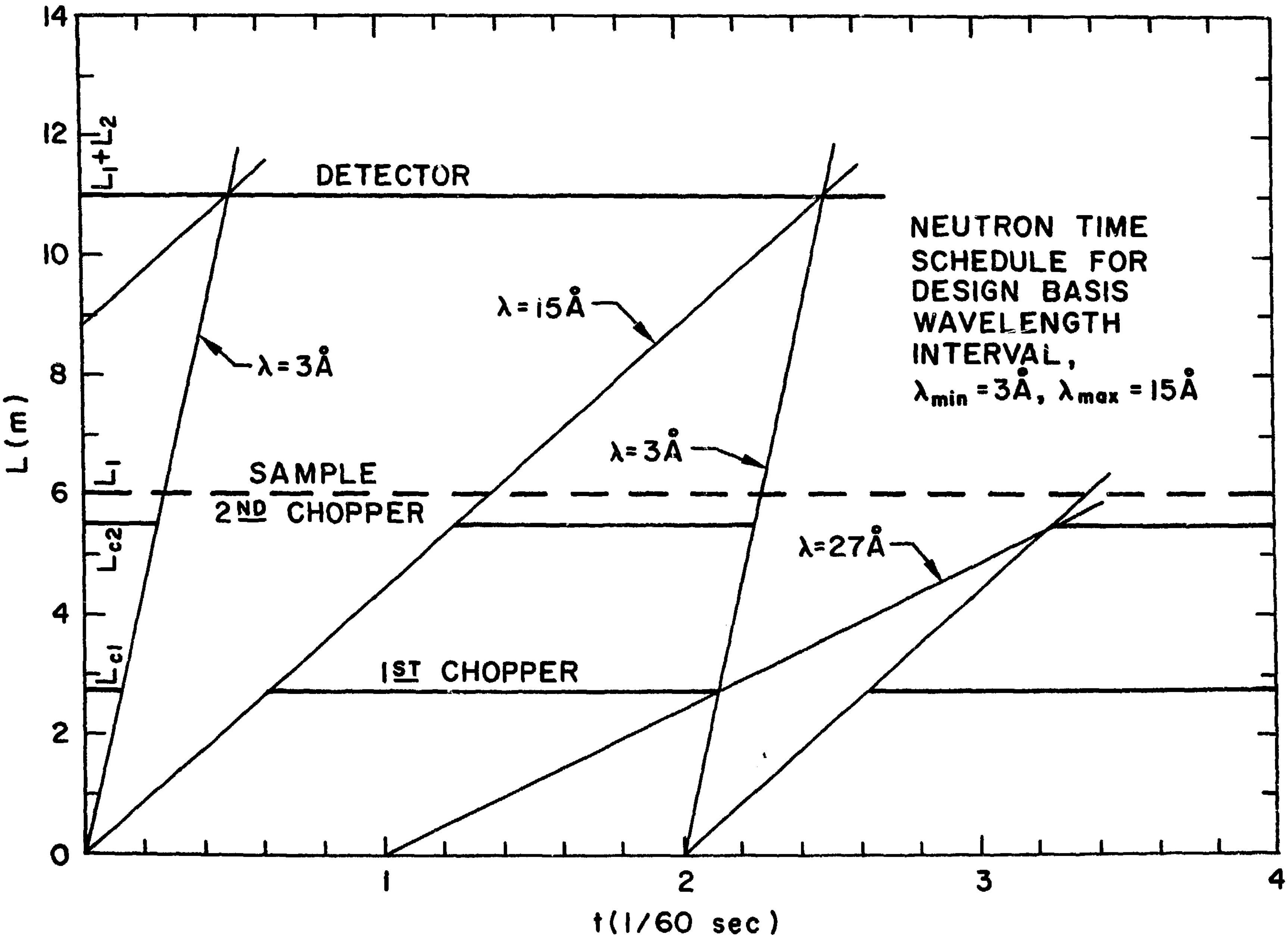

NEUTRON TIME SCHEDULE FOR DESIGN BASIS WAVELENGTH INTERVAL,
λmin = 3Å, λmax = 15Å
DETECTOR
SAMPLE
2ND CHOPPER
1ST CHOPPER
λ = 3Å
λ = 15Å
λ = 3Å
λ = 27Å
L1+L2
L1
Lc2
Lc1
L (m)
t (1/60 sec)
0
2
4
6
8
10
12
14
1
2
3
4

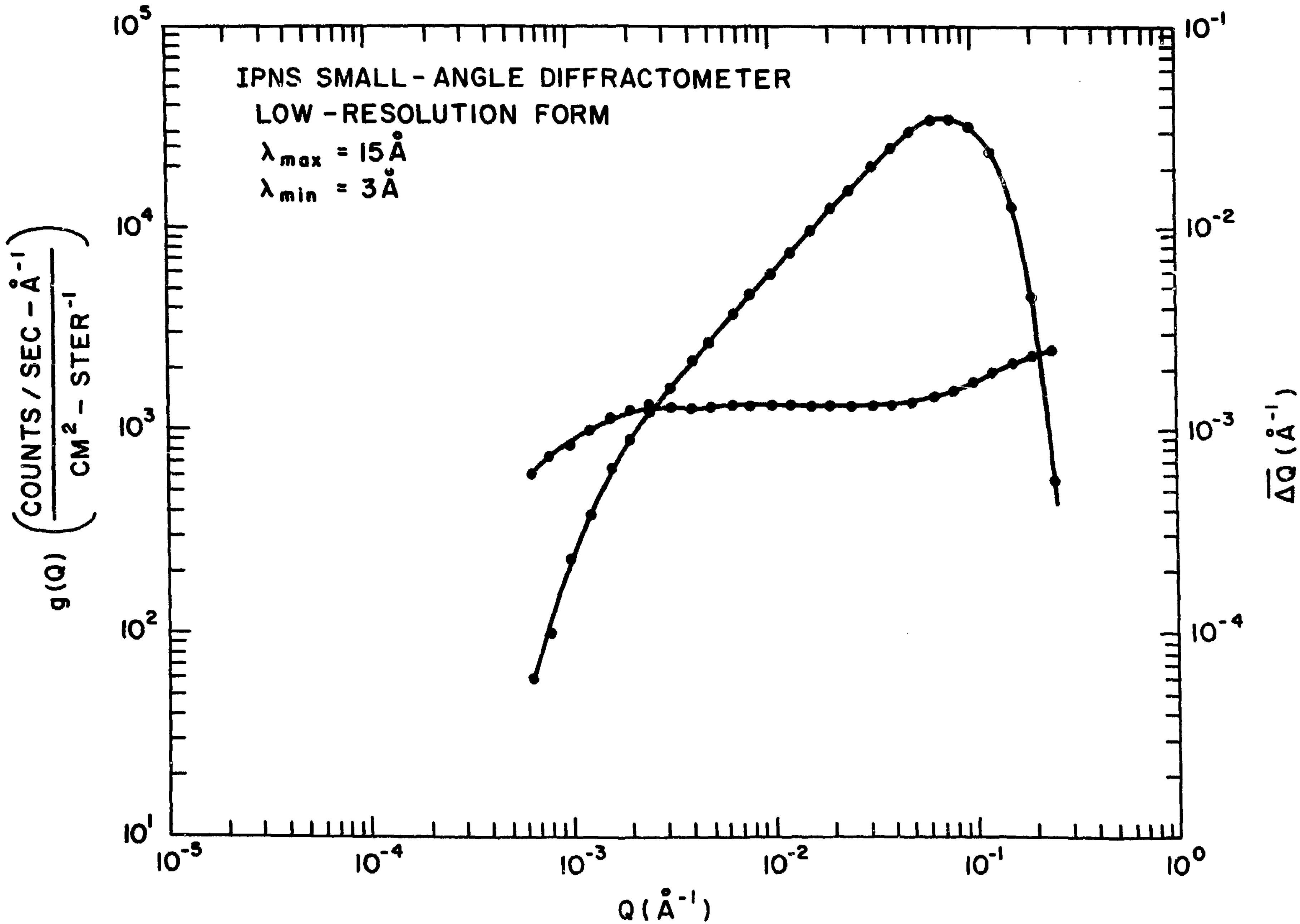

IPNS SMALL-ANGLE DIFFRACTOMETER
LOW-RESOLUTION FORM
λmax = 15 Å
λmin = 3 Å
g(Q) (COUNTS / SEC - Å⁻¹ / CM² - STER⁻¹)
ΔQ (Å⁻¹)
Q (Å⁻¹)
10⁵
10⁴
10³
10²
10¹
10⁻¹
10⁻²
10⁻³
10⁻⁴
10⁻⁵
10⁻⁴
10⁻³
10⁻²
10⁻¹
10⁰

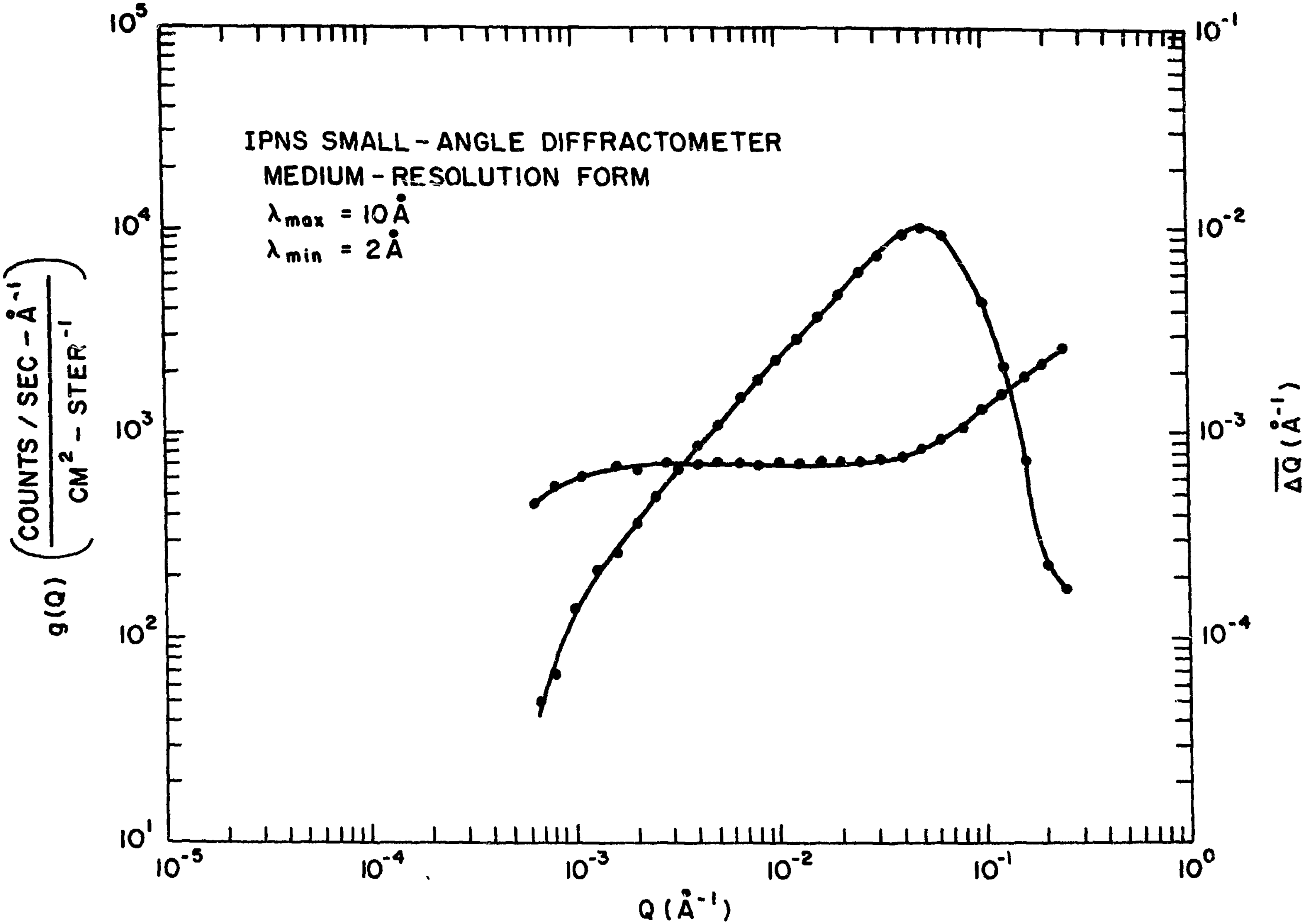
IPNS SMALL-ANGLE DIFFRACTOMETER
MEDIUM-RESOLUTION FORM
λ_{max} = 10 Å
λ_{min} = 2 Å
10^5
10^4
10^3
10^2
10^1
10^{-1}
10^{-2}
10^{-3}
10^{-4}
10^{-5}
10^{-4}
10^{-3}
10^{-2}
10^{-1}
10^0
Q (Å^{-1})
g(Q) (COUNTS / SEC - Å^{-1} / CM^2 - STER^{-1})
$\overline{\Delta Q}$ (Å^{-1})